J Electroceram (2009) 22:395–404
DOI 10.1007/s10832-008-9443-0

# Crystallographic and dielectric properties of highly oriented $BaTiO_3$ films: Influence of oxygen pressure utilized during pulsed laser deposition

**J. Hiltunen · D. Seneviratne · H. L. Tuller · J. Lappalainen · V. Lantto**

Received: 24 May 2007 / Accepted: 11 February 2008 / Published online: 8 March 2008
© Springer Science + Business Media, LLC 2008

**Abstract** The crystal structure of $BaTiO_3$ thin films grown by pulsed laser deposition on MgO substrates was found to be strongly influenced by the oxygen pressure used during growth. Low pressures produced epitaxial films with highly strained out-of-plane lattice parameter *c* compared to in-plane parameter *a*, while increasing oxygen pressure resulted in the ratio $c/a<1$ with a concomitant increase in polycrystallinity. The dielectric properties varied with changing crystal structure reaching a maximum permittivity value in films near the minimum point of tetragonal distortion and exhibiting relaxor-like behavior in $c/a<1$ films close to this point. Hysteresis observed in dielectric tuning loops pointed to the presence of the ferroelectric phase in all films at room temperature. As a result of high electric field poling treatment at 300 °C, the tunability generally increased and initially symmetric tuning curves became asymmetric. The tuning curve in $c/a<1$ samples became nearly linear, supporting the premise of polarization reorientation with changing deposition condition. Phase transitions to the paraelectric phase were highly suppressed and shifted upwards in temperature from the bulk transition temperature of 130 to ~250 °C in strongly *c*-oriented films. Moderate shifts in oxygen working pressure were demonstrated to produce films with very different properties thereby offering convenient means for strain engineering and control of preferred crystal orientation and polarization direction of highly oriented BTO films.

**Keywords** $BaTiO_3$ · Phase transition · Thin film · Stress · Strain

J. Hiltunen · D. Seneviratne · H. L. Tuller
Department of Materials Science and Engineering,
Massachusetts Institute of Technology,
77 Massachusetts Avenue,
Cambridge, MA 02139, USA

J. Hiltunen (✉)
Technical Research Centre of Finland,
Kaitovayla 1,
90571 Oulu, Finland
e-mail: jussi.hiltunen@vtt.fi

J. Lappalainen · V. Lantto
Microelectronics and Materials Physics Laboratory,
University of Oulu,
P.O. Box 4500, 90014 Oulu, Finland

## 1 Introduction

Ferroelectric materials have been intensively studied because of their functional properties, such as, relatively high and nonlinear permittivity, remanent polarization, piezo and electro-optic response offering opportunities for a wide variety of microelectronics and photonics applications [1, 2]. In thin film form, ferroelectrics are subject to stress, crystal orientation effects as well as a range of lattice defects [3–5]. As a result, many of the vital physical properties of perovskite ferroelectric films commonly differ from bulk values. While these properties are often degraded, they are in some cases enhanced, such as the increased remanent polarization in strained $BaTiO_3$ (BTO) films and room-temperature ferroelectricity in $SrTiO_3$ (STO) resulting from substrate induced stress [3, 6].

BTO commonly serves as the model perovskite ferroelectric [7]. The paraelectric (cubic) to ferroelectric (tetragonal) phase transition in bulk crystalline BTO occurs at 130 °C resulting in the onset of spontaneous polarization and the change from the cubic to the distorted tetragonal crystal structure [8]. Both experimental and theoretical

studies show that significant increases in the phase transition temperature may result from strains induced by lattice mismatch or thermal expansion difference between the epitaxial film and substrate [3, 9–16]. Furthermore, theoretical first-principle [13, 15] and thermodynamic [10, 14] studies suggest that the room temperature phase need not necessarily be tetragonal, with other phases possible, depending on the amount of stress and its character i.e., tensile or compressive.

One demonstrated means for tuning the lattice parameter of perovskite thin films is to vary the oxygen partial pressure during film growth [17–23]. Deposition kinetics [17] and the resultant stoichiometry [22] of the grown films have been proposed as explanations for this phenomenon. The tunability of the lattice parameter utilizing this method has been applied e.g. in pulsed laser deposition [20] (PLD) and sputtering [17] processes. As a result of the shift in lattice parameter mismatch between film and substrate, the stress state can be changed. This, in turn, can result in a change in preferred orientation [17, 18, 20, 22, 23] and even the crystal phase of the film, e.g., the paraelectric or ferroelectric phase, depending on working pressure [24].

In this paper, we report on the role of oxygen partial pressure during PLD growth in influencing BTO thin film crystal structure and how permittivity is modified with changing crystallographic properties. Also an examination of how these factors influence the ferroelectric to paraelectric transition at elevated temperature is included in this work. This article is divided in the following manner. After summarizing methods used in sample preparation and characterization, the results and analysis are presented. First, the role of process conditions on crystallographic properties is presented including crystal phase identification and orientational issues together with the in-plane and out-of-plane lattice parameter determination. Along these lines, surface morphology is examined to identify changes in crystal growth mechanism, and from a technological point of view, to estimate the suitability of the films in applications where surface roughness is an important factor. Second, the room temperature permittivity and its non-linearity is examined. Permittivity is often electric field direction sensitive due to the BTO's ferroelectric nature while also being affected by the stress level in the films. Electrical measurements are used to illuminate how shifts in crystallographic properties suggested by XRD analysis are transferred to permittivity. The temperature dependence of the permittivity and lattice parameters were also examined to provide insight on how in the ferroelectric to paraelectric phase transition may be influenced by stress levels thereby offering further insight into the strength of substrate clamping. Finally, the results are summarized with concluding remarks.

## 2 Experimental

Highly oriented BTO thin films were grown onto single crystal MgO substrates with (001) orientation by the PLD method. The deposition system was equipped with a KrF (248 nm) excimer laser with its beam focused onto the nominally stoichiometric $BaTiO_3$ pressed and sintered target. All films were grown by using a laser repetition rate of 5 Hz and fluence of 2.5 J/cm$^2$. The substrates were heated to 700 °C before depostion with oxygen partial pressure the only varied process parameter. Oxygen pressures of 1.5, 10, 15, 20, 25 or 30 mTorr were applied during each deposition. The measured film thickness of each sample was 306, 356, 389, 475, 468 and 395 nm with increasing oxygen pressure. Repeated thickness measurements produced the standard deviation of 3%. The crystal structure was examined by x-ray diffraction (XRD) measurements. First, a Rigagu RU 300 diffractometer was used in $\theta$–$2\theta$ scans at room temperature to characterize the crystal phases and preferred orientation. The out-of-plane lattice parameter of the BTO films was calculated from the peaks in the $\theta$–$2\theta$ pattern. This was followed by mapping of the non parallel-to-surface planes (Bruker D8 equipment) to identify the symmetry of the crystal planes and to calculate the in-plane lattice parameter with the help of $\theta$–$2\theta$ scan results. Also, high temperature XRD studies were carried out with a Bruker D8 instrument. The XRD measurement error was minimized by use of MgO substrate peaks as internal standards in the diffraction scans. Changes in film surface morphology were tracked by atomic force microscope (AFM), Nanoscope III. A micro-probe station, equipped with a small heater and an HP 4192A impedance analyzer, was utilized in the dielectric measurments. Relative permittivity and its tunability, i.e. change in permittivity as a function of applied bias electric field, were characterized with an platinum inter-digital-electrode (IDE) configuration, which was sputter deposited onto the film and lift-off patterned. The error in permittivity due to geometrical variation of electrodes was estimated by fabricating IDE capacitors with 10 μm (52 fingers) and 20 μm (26 fingers) widths and separation and length of 800 μm. By using Farnell's analysis (described and utilized e.g. in Ref. [25].) and applying a stray circuit model to take into account a finite impedance of cables, probes and electrodes, less than 9% deviation was observed in permittivity obtained with different electrode configurations on the same film. Prior to dielectric measurements, the electroded samples were heated to 500 °C and cooled to room temperature to avoid potential electrode destabilization effects during actual measurements. The sample temperature was monitored by a thermocouple attached to the sample during elevated temperature permittivity studies.

## 3 Results and discussion

### 3.1 Crystal structure and morphology analysis

Figure 1 shows the XRD $\theta$–$2\theta$ measurement of the BTO films deposited at different oxygen pressures. Only the (001) peak and its multiples were observed in the thin films grown at a gas pressure ≤10 mTorr. The diffraction peaks of the thin film shifted towards lower diffraction angle compared to characteristic bulk BTO (00m) positions, implying enlargement of out-of-plane lattice parameter compared to the corresponding bulk *c*-axis value. As the oxygen pressure was increased, the main peaks shifted between the characteristic bulk single crystal BTO (00m) and (m00) positions. This indicates a change in preferred orientation from (001) to (100) orientation. This crystal reorientation was verified by the tilted-angle XRD measurements described below. When the oxygen pressure exceeded 15 mTorr, reflections from (110)/(101) oriented planes were also observed in the $\theta$–$2\theta$ pattern together with (m00) main peaks indicating a change from hetero epitaxial film to a polycrystalline structure. As the oxygen pressure reached 25 mTorr, minor non-characteristic tetragonal BTO phases were also observable in the $\theta$–$2\theta$ pattern when plotted on a log-scale. It is also interesting to notice that asymmetric peaks may imply non uniform microstrains in the films. Analysis of the $K\alpha_2$ radiation removed pattern revealed that, in films deposited at 1.5 and 10 mTorr, when the peak angle is shifted to lower angle relative to the bulk reflection position, the peaks are more spread to higher angles towards the characteristic *c*-axis peak position. The 15 mTorr sample has the most symmetric peaks, indicating uniform stress level. The films deposited at 20, 25 and 30 mTorr are non-symmetrically spread towards the lower angle. Related strains have also been observed in Pb $(Zr_xTi_{1-x})O_3$ films experiencing shift in preferred orientation as a function of film thickness and having the highest level of microstrain in *a*-axis oriented films near the reorientation point and local minimum in microstrain on the *c*-side of the reorientation point [26].

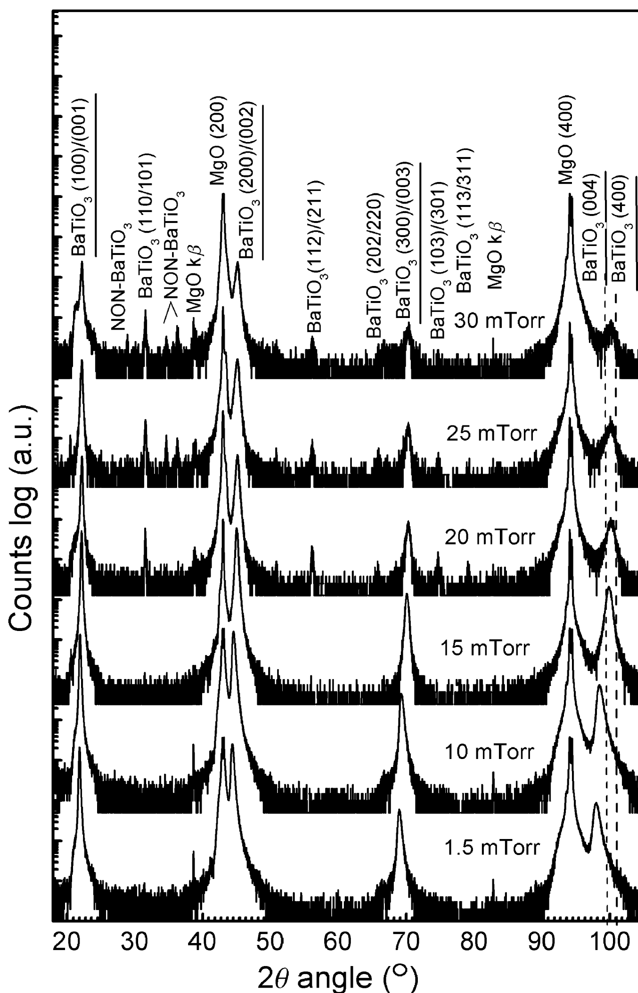


**Fig. 1** X-ray diffraction $\theta$–$2\theta$ measurement of $BaTiO_3$ films deposited at different oxygen pressures. *Dashed lines* near 100° angle represent free bulk $BaTiO_3$ (004) and (400) reflections at room temperature. *Underlined* labels represent the (00 m)/(m00) reflections, which are from the preferred orientation planes in $BaTiO_3$ films

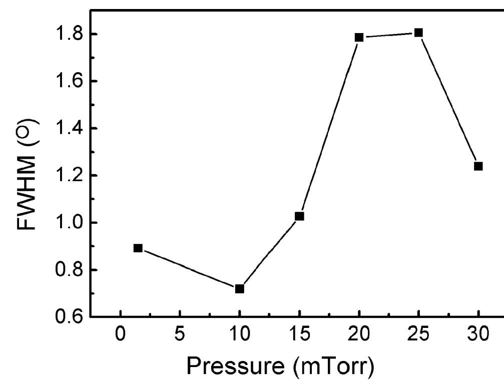


**Fig. 2** Rocking curve FWHM values of the (002)/(200) $BaTiO_3$ reflection as a function of oxygen pressure during deposition

Figure 2 shows the full width at half maximum (FWHM) values of the rocking curves of the (002)/(200) reflections as a function of oxygen pressure during deposition. A value of about 1° FWHM in samples deposited at 1.5–15 mTorr oxygen pressure implies relatively good substrate constrained film crystal growth. It has been shown that the rocking curve FWHM value is film thickness sensitive, decreasing with increasing film thickness, due to a partly misaligned BTO film near the film–substrate interface [27]. Rather similar FWHM values, compared to results in this work, were characterized for PLD prepared thin films in Ref. [27] with approximately the thickness of 200 nm. When the pressure exceeded 15 mTorr, the FWHM value increased and reached a maximum value in 20 and 25 mTorr films close to the point when *a* exceeds the *c* parameter.

This behavior can be attributed to the change from hetero-epitaxial to textured structure. The same trend was observed also in $\varphi$-scan measurements of (103)/(301) planes when samples were rotated by 360° (Fig. 3). Each sample showed fourfold symmetry along the MgO main crystal direction. In the films deposited at oxygen pressure of 1.5, 10 and 15 mTorr, the intensity between peaks was very low, further indicating the hetero-epitaxial film structure. When the oxygen pressure was 20 mTorr or higher, the films were textured. Peaks were broader and a slight intensity remained at all $\varphi$ angles presumable due to randomly oriented grains between the substrate aligned columns. For the 30 mTorr sample, the peaks became sharper, correlating with rocking curve measurements, and indicating a stronger influence of substrate on film crystal orientation.

Figure 4 shows the variation of the lattice parameters together with the measurement associated error bars as a function of the oxygen pressure during film growth. Out-of-plane values were calculated from the $\theta$–$2\theta$ patterns and in-plane parameters from the off-axis reflections (202)/(220) together with the calculated out-of-plane values. As the gas pressure increases, the out-of-plane lattice constant decreases. At low oxygen pressures the lattice constant was significantly larger than that of the BTO single crystal $c$=4.038 Å (Ref. [28].). The $c$-axis values of 4.09 and 4.07 Å were determined for the films deposited at the oxygen pressure of 1.5 and 10 mTorr, respectively. Highly strained $c$-axis oriented polycrystalline BTO films have been reported also in Ref. [17], in which a near 4.20 Å $c$-axis was reported. Also epitaxial BTO films with $c$-axis orientation can possess a significantly shifted out-of-plane axis from the bulk crystalline BTO value when grown on various substrates [3, 4]. It was also shown that the in-plane lattice constant does not necessary differ remarkably from the corresponding bulk value with fluctuating out-of-plane parameter. This was also observed in this study in the samples deposited at low oxygen pressure, where the in-plane lattice parameter was close to the free BTO crystal value. The region in Fig. 4 between 15 and 20 mTorr is particularly interesting since it reflects the oxygen pressure range where the $c/a$ ratio decreases below 1. A similar shift of $Ba_xSr_{1-x}TiO_3$ (BST) films on MgO substrates has also been reported nearly reaching the cubic phase at a specific oxygen pressure [22–24]. Preferred orientation of sputter deposited BTO thin films on amorphous quartz, with changes from (100)/(001) to (110) with increasing process pressure [17] has also been observed.

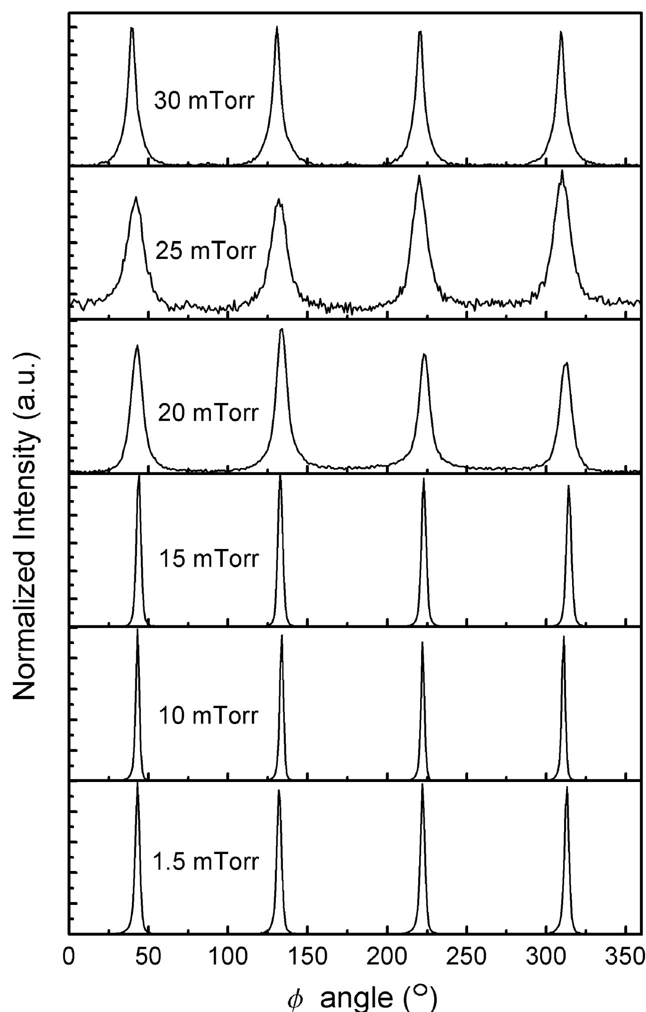


**Fig. 3** X-ray diffraction $\varphi$-scans of (103)/(310) reflections of $BaTiO_3$ thin films deposited at different oxygen pressures

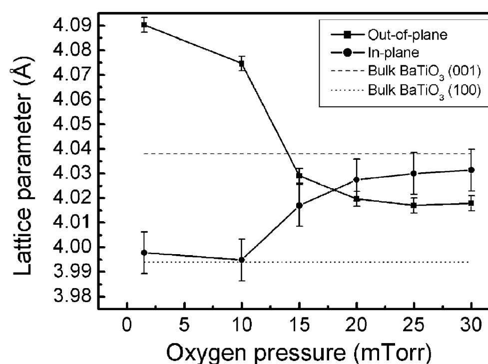


**Fig. 4** Out-of-plane and in-plane lattice parameters of $BaTiO_3$ films as a function of oxygen pressure during deposition

The identity of crystal phase in coherent hetero-epitaxial films has recently attracted much theoretical interest. Although some controversy remains with respect to the nature of the detailed temperature dependent strain-phase diagram, agreement exists that substrate induced compressive biaxial stress favors the tetragonal $c$-phase with polarization vector along the <0,0,±1> substrate direction (for example, Ref. [14]). Near the strain free region, the ferroelectric $r$-phase is monoclinic and the polarization vector points to the <$n$,$n$,$m$> crystal direction. Under tensile biaxial stress, the coherent epitaxial film is in the $aa$-phase

(orthorhombic) with polarization vector along the <±1, ±1,0> direction. In this study, the high pressure films were not epitaxial, though highly oriented, given observed minor (110)/(101) peaks in the $\theta$–$2\theta$ XRD scans together with lack of non-zero intensity between the peak angle in the $\varphi$-scans. Therefore, it is expected that the substrate influence was partly relaxed due to the polycrystalline structure. In off-axis measurements of the $c/a<1$ films, i.e. the elongated unit cell axis is along the surface, reflections from (202) and (220) planes were undistinguishable. A similar lack of tetragonal peak splitting is reported for the epitaxial *a*-axis oriented BTO films on single crystal MgO substrate [12]. This was attributed to a slightly different orthorhombic phase in the film from the orthorhombic phase in the bulk. In the film, the pseudocubic phase has a square in-plane lattice due to substrate constraint, while in the bulk, the unit cell is elongated along the face diagonal direction [12]. This is also possibly the case in this work, though 20–30 mTorr films were not epitaxial according to the $\theta$–$2\theta$ and $\varphi$-scans presumably due to randomly oriented grains between the substrate aligned columns. If coherent epitaxy is maintained without crystal defects, then the phase would follow the $c \rightarrow r \rightarrow aa$ chain along with increasing oxygen pressure during deposition. Though the crystal phase of the films can not be determined conclusively in this work, this trend is observed based on the XRD measurements and also supported by the electrical measurements described below. Potentially, 1.5 and 10 mTorr samples are *c*-phase, while the 15 mTorr sample is closer to the *aa*-phase possessing either the *c*- or *r*-phase. Further pursuit of the phase evolution is unclear due to breakdown of epitaxy and induced growth of non-characteristic BTO phases, but the tendency for in-plane elongated lattice is observed with high oxygen pressure.

Several mechanisms have been suggested to affect the change in crystal phase and lattice constant, such as, (1) deviation in stoichiometry [18, 22], (2) lattice mismatch [3, 4] and (3) different thermal expansion between substrate and film [27, 29], (4) kinetic energy [17] and the (5) directional distribution of particles [17] during vacuum deposition. Strain due to lattice mismatch between film and substrate changes the lattice parameter of films, especially, when epitaxial thin films are grown on near lattice-matched substrates in which large intrinsic strains are created by the film lattice attempting to follow the substrate lattice periodicity. As a result, strain-induced structural change can have a significant effect on the film structural properties. Furthermore, strain due to the thermal expansion difference between the film and substrate also alters the structure of the deposited film during cooling from the deposition temperature to room temperature. For example, it was estimated that during the cooling process from 700 °C to room temperature, the parallel to substrate surface strain is −0.28% between BTO film and MgO substrate [29]. This can put BTO under compressive stress for the in-plane directions and favors a condition where the *c* axis of the BTO in the tetragonal phase aligns itself perpendicular to the surface [27, 29]. The lattice of an oxygen deficient perovskite film expands beyond that of the corresponding bulk ceramic [22] as a result of the shifted nearest neighbor distance due to the reduced Coulomb attractive force between cations and anions in an oxygen deficient lattice. In Ref. [21] oxygen pressure effects on homo-epitaxial ($SrTiO_3$ film on $SrTiO_3$ substrate) during pulsed laser deposition was studied to avoid substrate influence on the film lattice parameter. It was found that the out-of-plane lattice parameter shifted along with the oxygen pressure, confirming that lattice parameter shift is not only a substrate originated effect. Oxygen vacancies are also proposed as a mechanism for affecting the internal stress state change in perovskites (from tensile to compressive with decreasing oxygen pressure). This is attributed to substrate–film lattice mismatch induced stabilization of crystallographically different oxygen vacancy sites; (0, 1/2, 1/2) vs (1/2, 1/2, 0) [22].

Figure 5 shows an AFM image of the surface of each sample and in Fig. 6 the corresponding RMS surface roughness values. At low oxygen pressure, the surface is

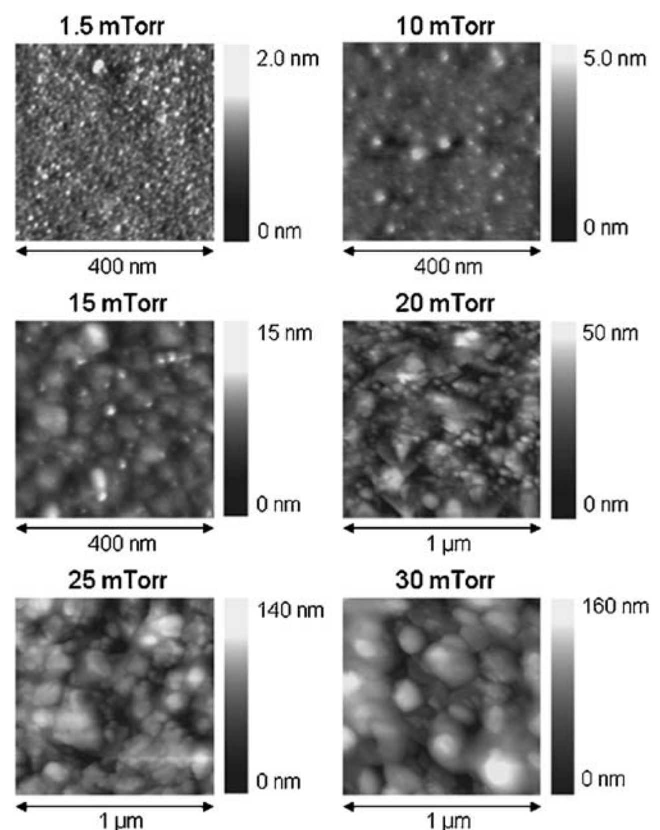


**Fig. 5** AFM images of film surface morphology as a function of growth atmosphere

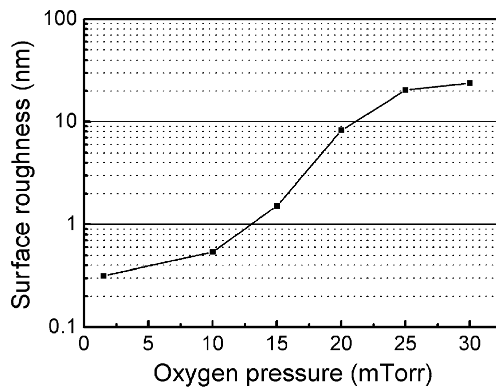


**Fig. 6** RMS surface roughness as function of working pressure during deposition determined by AFM measurements

smooth with a RMS surface roughness value of unit cell order. The 10 mTorr oxygen pressure deposition condition produced a film having a generally smooth surface with a bimodal microstructure. As the pressure was further increased, the RMS surface roughness value increased sharply when the oxygen pressure exceeded 15 mTorr but then plateaued in the 25 nm range at high deposition pressure. These measurements together with XRD measurements indicate a change in the film growth mechanism from epitaxial towards polycrystalline.

### 3.2 Room temperature dielectric properties

The measured 1 MHz dielectric constant is plotted in Fig. 7 as a function of the oxygen pressure used during deposition. A 1.5 mTorr sample had a room temperature relative permittivity of 470. The maximum relative permittivity of 620 was measured for the 15 mTorr deposited sample. The initial increase in permittivity at low oxygen pressures can be attributed to the relaxation of strongly clamped *c*-phase with partly relaxed crystal stress due to defects, e.g. dislocations, which can also be observed in increased FWHM rocking curve values for the (002) reflection in Fig. 2. As the pressure exceeds 15 mTorr, and the $c/a$ ratio is <1, relative permittivity decreases by nearly 50%. The trend correlates with the bulk BTO direction dependent relative permittivity of $\varepsilon_{11}$=2,200 and $\varepsilon_{33}$=56, where the latter value corresponds to the geometry in which the applied electric field lies along the polarization vector direction while the large value corresponds to the case in which the field is perpendicular to the polarization vector [30]. The decrease in net polarizability is partly a result of the reduced crystal quality, in which the relative grain boundary volume is increased thereby reducing the average dielectric constant. Rather similar trends in oxygen working pressure depended relative permittivity are reported for PLD processed BST films. For the $Ba_{0.5}Sr_{0.5}TiO_3$ composition, the highest permittivity value was measured for a film with the lowest distortion from the cubic crystal phase as also observed in this work [22]. In $Ba_{0.4}Sr_{0.6}TiO_3$ films [24], peaking in the permittivity was attributed to the paraelectric–ferroelectric phase transition, which was induced by oxygen working pressure dependent strain in the film, while in the stoichiometric bulk material, this composition is paraelectric. It is worth noting that, in the IDE configuration, both the vertical and horizontal electric field components are induced in the capacitor structure and their ratio, together with the crystallographic orientation of the film, determines the measured net effect.

Figure 8 shows the normalized tunability of the relative permittivity as a function of electric field, i.e. $E$=voltage/(IDE finger separation). During measurements, electric fields up to 3.4 V/μm were applied with no observation of tunability saturation. The 1.5 mTorr sample had a tunability of 5% at maximum field with slight hysteresis. The highest tunability of 9% was measured for the 10 mTorr sample. A tunability of 6% was observed in the 15 mTorr sample which exhibited a unique tunability curve characterized by the most open hysteresis loops and a clear increase in dielectric constant at small electric fields. This may be explained by domain re-orientation under external applied field. The slope at high field was similar to the exhibited by the 10 mTorr sample. The hysteresis loops of the samples deposited at 20, 25, 30 mTorr, i.e. $c/a$<1, had nearly identical tuning curves, i.e. a field insensitive region at low fields and ~5% tunability at maximum applied field with limited hysteresis.

To confirm the existence of the ferroelectric phase and to study the effect of poling on dielectric tunability, the samples were heated to 300 °C with a DC electric field of 8 V/μm applied across the IDE finger pairs during the cooling phase. The symmetric tuning curves before poling became asymmetric and generally the tunability increased (see Fig. 9). Samples deposited at 1.5 and 10 mTorr pressures exhibited 5% and 10% tunability opposite to and along the poling electric field directions, respectively. The 15 mTorr sample had a ~15% tunability in both directions. Along the poling direction, the hysteresis loop opening was

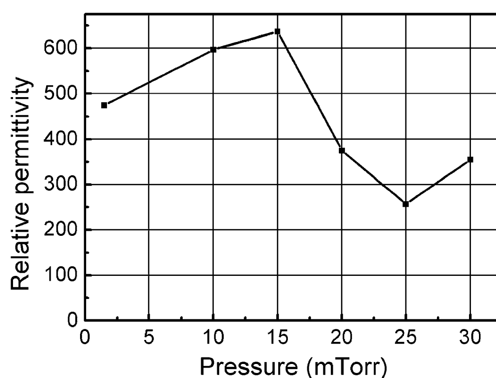


**Fig. 7** Room temperature dielectric constant at 1 MHz in $BaTiO_3$ films as a function of oxygen pressure during deposition

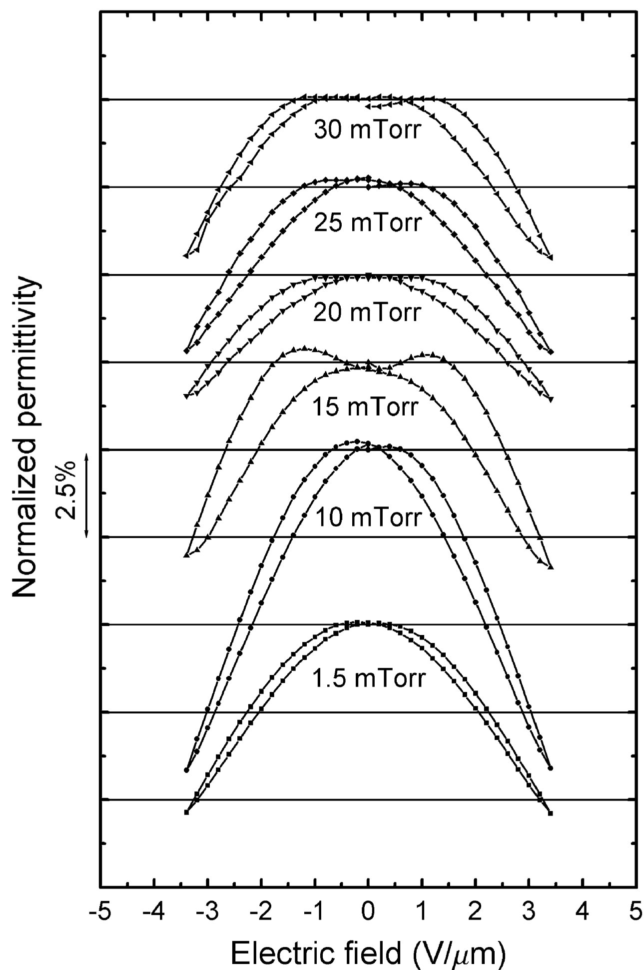


**Fig. 8** Normalized relative permittivity at 1 MHz as function of bias field measured in $BaTiO_3$ films deposited at different oxygen pressure

very narrow, but opened considerably in the opposite direction. The samples deposited at 20, 25 and 30 mTorr also showed asymmetric behavior after poling. The tuning curve along the polarizing field was linear with a slight hysteresis and in the opposite direction, the dielectric constant plateaued at 5% tunability. Generally, the poling slightly polarized the $c/a>1$ films while the tuning curves for $c/a<1$ films became nearly linear as a result of this treatment. The strong effect of poling on the 15 mTorr sample supports the assumption that it also has a polarization component along the surface, i.e. it can potentially be in the *r*-phase as also supported by reduced tetragonality according to XRD measurements. High dielectric tunability close to point with low lattice distortion from cubic symmetry has also been reported for BST films, correlating well with results obtained in this study [24].

### 3.3 Phase transition studies at elevated temperatures

The displacement of ions in the lattice from a centrosymmetric cubic state to a non-centrosymmetric tetragonal state results in the onset of spontaneous polarization in bulk BTO crystals at ~130 °C. This is reflected as a first order change from spontaneous polarization Ps=0 in the paraelectric phase to Ps>0 in the ferroelectric phase [8]. As the temperature is further decreased, additional ferroelectric transitions occur upon transitions to lower symmetry orthorhombic ($T$=0 °C) and rhombohedral ($T$=−90 °C) phases, respectively. These transitions are accompanied, in bulk samples, by rapid changes in lattice parameters and dielectric constant. These phase transitions in films can be broadened, suppressed or shifted to higher temperature depending on the magnitude and nature of stress that the films experience. One explanation for a broadened transition is that the film is not structurally and/or chemically homogeneous across its thickness, which could lead to strain gradients that would eventually broaden the transitions [31]. Furthermore, in Refs. [32] and [33], it was shown that temperature dependent anomalies of permittivity and lattice parameter in BST films are thickness dependent. In the case of single crystals or coarse grained ferroelectric bulk ceramics, the first order phase transition from ferroelectric to paraelectric phase, or vice versa, takes place abruptly at the Curie temperature $T_c$ in the whole

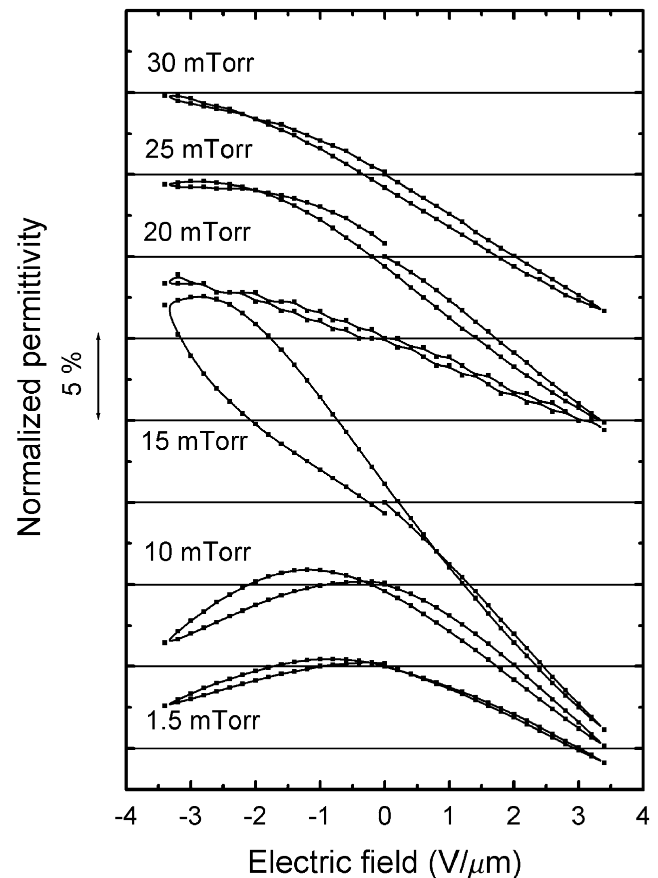


**Fig. 9** Normalized relative permittivity at 1 MHz after poling treatment as a function of bias field measured in $BaTiO_3$ films deposited at different oxygen pressure

volume of the material. Order parameters like remanent polarization $P_r$, dielectric constant $\varepsilon_r$, and piezoelectric coefficients $k_{ij}$ increase steeply and reach a sharp maximum at $T_c$. However, when a material's microstructure is nonideal, for example, large numbers of defects or dislocations, very small or nonuniform grain size, long range chemical composition variations, or the material is under macroscopic or microstress, the phase transition temperature $T_c$ also varies as a function of these properties and may have a distribution across the material volume. Thus, the transition initiates within small volumes units at many different locations characterized by the lowest transition temperature, and slowly expands across the whole sample by sequential transitions in appropriate volume units with increasing temperature. This induces an increase in apparent order parameter, i.e. a broadened transition with shifted and moderate maximum values in comparison to single crystal or bulk ceramics.

The real and imaginary components of the relative permittivity of BTO films grown at different oxygen pressures are plotted in Fig. 10 as a function of temperature. Each plot shows these parameters measured at frequencies of 100, 158, 251, 398, 630 and 1,000 kHz (arrows show direction of increasing frequency). In all cases, the real part of the relative permittivity remained above ~200–400 and reached values as high as ~275–700. The low pressure grown samples (1.5 and 10 mTorr) did not show the characteristic phase transition related peak in the real part of relative permittivity either at the bulk value of ~130 °C or at elevated temperatures up to the maximum measurement temperature of this study, 400 °C. This would imply the lack of phase transition from ferroelectric (as suggested by permittivity tuning and poling experiments) to paraelectric phase due to high stress levels in the film. As the oxygen pressure exceeded 10 mTorr, the characteristic peak was observed in the general vicinity of ~100–150 °C, although suppressed, compared to the single crystal first-order transition. The BTO film deposited at 15 mTorr had reduced tetragonality, and possibly less clamped by the substrate, compared to the highly *c*-oriented samples, which can explain the observed dielectric properties at elevated temperatures. Films deposited at high oxygen pressure ($c/a$ <1) were polycrystalline according to the XRD measurements, which clearly reduces the substrate effect on the phase transition. All of them showed the characteristic, but suppressed, BTO phase transition feature in the real part of relative permittivity near the transition temperature in bulk BTO. Although no clear evidence of a phase transition was evident in the real part of the relative permittivity of the samples with strongly elongated *c*-parameter, a clue to such transition can be obtained by examining instead the imaginary part. 1.5 and 10 mTorr oxygen pressure grown samples exhibited broad peaks between ~250 and 350 °C

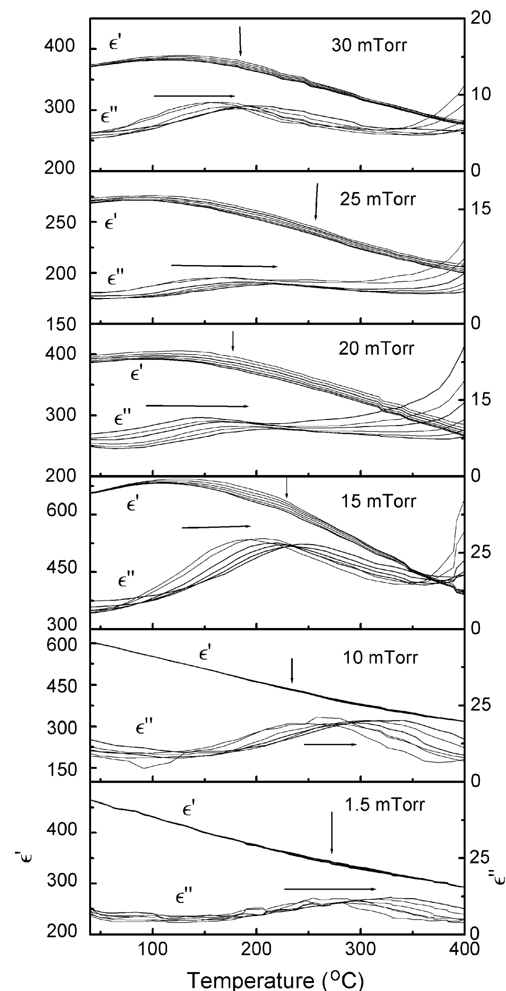


**Fig. 10** Real $\varepsilon'$ and imaginary $\varepsilon''$ parts of the relative permittivity as a function of temperature in $BaTiO_3$ films deposited at different oxygen pressure. *Arrows* represent the direction of increasing frequency (100→1,000 kHZ)

depending on the measurement frequency. Peak temperatures were considerably lower in the specimens grown at higher oxygen pressures with values more typically in the range of 150–230 °C depending on frequency. This suggests that *c*-oriented films experience the ferroelectric-paraelectric phase transition at considerably higher temperatures than free BTO bulk crystals. On the other hand, *a*-oriented samples deposited at 20, 25 and 30 mTorr, appear to exhibit phase transitions much closer to that of bulk BTO.

Further information related to the phase transition can be obtained by examining the frequency dispersion in the real part of relative permittivity in greater detail. Such relaxor like behavior as observed here is also observed in epitaxial BTO and BST films at low temperature phase transitions as a consequence of possibly randomly distributed polar clusters [34]. In highly *c*-oriented samples, the real part, $\varepsilon'$, showed only a slight frequency dispersion at temperature range between 200 and 350 °C. This, together with peaking in $\varepsilon''$, support the hypothesis that the shift towards higher

temperatures of the onset of the phase transition in the 1.5 and 10 mTorr prepared samples is due the substrate clamped *c*-phase. While the frequency dispersion in $\varepsilon'$ was low in the 15 mTorr sample at the two extremes of temperature, it became more evident over the intermediate temperature range presumably due to the broadened phase transition. The 20 and 25 mTorr prepared specimens showed frequency dependence at all temperatures while the 30 mTorr prepared specimen had a rather similar character to that of the 15 mTorr sample with the highest frequency dispersion near the likely phase transition point. This points to polar clusters driving the relaxational nature of the polycrystalline films (20 and 25 mTorr) and the more characteristic ferroelectric behavior in the 15 and 30 mTorr films. This is also supported by the phi-scan XRD measurement (see Fig. 3), where the crystal structure of the $c/a>1$ films (oxygen pressure of 1.5–15 mTorr) and 30 mTorr grown films is more aligned by the substrate lattice.

Given the unique features of films deposited at 10 and 15 mTorr, i.e. epitaxial films with different lattice constant and different suppression level in the real part of permittivity, the apparent phase transitions of these samples, suggested by the peaks in $\varepsilon_r''$, were also studied by elevated temperature XRD measurements. Figure 11(a) shows the in-plane and out-of-plane lattice parameters of the samples deposited at 10 and 15 mTorr oxygen pressures at elevated temperature. Distortion from the cubic structure, defined as ratios between in- and out-of-plane parameters, are plotted in Fig. 11(b). The 10 mTorr prepared sample showed a linearly increasing lattice constant in both crystal directions and basically constant tetragonal distortion up to 230 °C. Above this temperature, tetragonality decreased monotonically with increasing temperature. In the vicinity of 230 °C, the above mentioned relaxor type frequency dispersion in the real part of the permittivity together with peaking of the imaginary part of permittivity were also observed. This suggests that the film, or part of it, can experience a highly suppressed phase transition and remains tetragonally distorted from the cubic structure. This transition is not necessarily first order as shown by high temperature second-harmonic-generation (SHG) studies [3] and ferroelectric *P–E* hysteresis loop measurements [11], but instead the characteristic ferroelectric properties diminish gradually over a wide temperature range. Recent experiments suggest also that epitaxial films can maintain tetragonality beyond the ferroelectric to paraelectric phase transition turn-on temperature [3, 12]. In the 15 mTorr prepared sample, the tetragonality instead decreased over a broad temperature range already beginning at room-temperature. Below 200 °C this was mainly due to an increase of *a*-axis lattice value with stable *c*-lattice parameter. The lower transition point in the 15 mTorr vs the 10 mTorr specimen is also supported by the decreased peaking temperature of the imaginary part of the relative permittivity in Fig. 10.

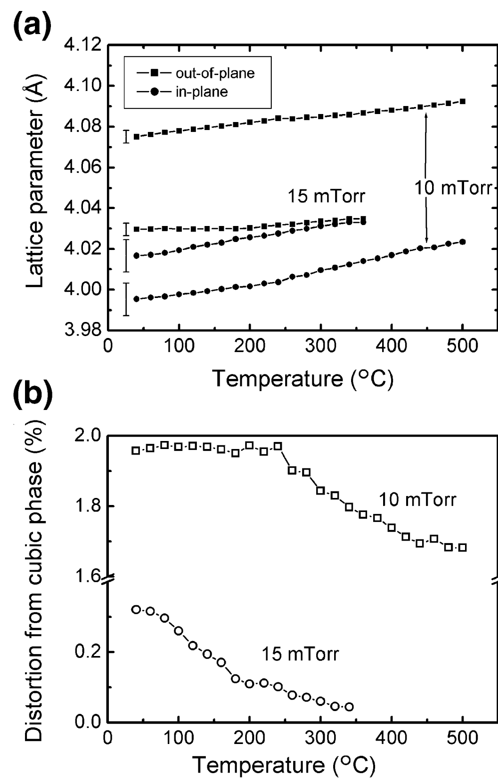


**Fig. 11** High temperature x-ray diffraction measurements. (**a**) In-plane and out-of-plane lattice parameters of $BaTiO_3$ films deposited at 10 and 15 mTorr. (**b**) Distortion from cubic phase defined as ratio between in-plane and out-of-plane lattice constants

## 4 Concluding remarks

Crystal orientation is known to be a significant factor in ferroelectrics due to direction sensitive responses (permittivity, electro-optic and piezo effect) in these polar materials. In thin film form, these materials are further susceptible to substrate clamping with additional important implications for properties. In this study, the crystal structure of BTO thin films grown on MgO single crystal substrates by PLD was found to be strongly influenced by the oxygen partial pressure used during growth. Low oxygen pressure favored films with $c/a>1$ and roughness only on the order of unit cell dimensions. With increasing oxygen pressure, the out-of-plane lattice parameter decreased, while the in-plane value increased resulting $c/a<1$ with a concomitant increase in polycrystallinity and surface roughness reaching levels of over 20 nm RMS, a value too high for e.g. optical devices.

The room temperature permittivity was found to be dependent on processing conditions with permittivity initially increasing as tetragonal distortion decreased and

reaching a maximum close to the point of low tetragonal distortion, the latter presumably a result of shift in stress level. $c/a<1$ oriented samples deposited at high oxygen pressure had a lower dielectric constant, which correlates with bulk directional properties and degraded crystal quality. The existence of the ferroelectric phase in these films was confirmed by the observation of hysteresis tuning loops in permittivity tuning measurements. This was further supported by the clear influence of poling on tuning behavior. The initially symmetric tuning curves became asymmetric especially in samples with $c/a<1$, in which the tuning curve became almost linear as a result of the main electric field component in IDE structure being applied along the polar plane. These observations in linear and non-linear permittivity confirm how significantly dielectric properties can be influenced by manipulation of polarization vector orientation.

The influence of stress level on the ferroelectric to paraelectric phase transition was studied by elevated temperature dielectric and XRD measurements. In samples with significantly elongated $c$ parameter deposited at low oxygen pressure, characteristic peaking of the real part of the permittivity was completely suppressed. Instead, peaking was observed in the imaginary part of the permittivity accompanied by relaxor type frequency dispersion, suggesting the formation of polar clusters. The samples deposited at higher oxygen pressure exhibited a somewhat suppressed and broadened transition in the vicinity of the bulk BTO transition point. These permittivity studies, supported by XRD measurements at elevated temperatures, show that both the nature and onset temperature of the phase transition and the dielectric properties are highly sensitive to processing parameters. Even moderate shifts in oxygen working pressure near the $c/a\approx1$ point (here, near 15 mTorr) were demonstrated to produce films with very different properties thereby offering convenient means for strain engineering of ferroelectric, dielectric and other polar sensitive properties of BTO and related perovskite structured films.

**Acknowledgements** The authors acknowledge the support from Analog Devices, Inc. J. H. acknowledges the financial support of the Academy of Finland and the Infotech Graduate School of the University of Oulu. The authors would also like to thank Prof. C. Ross for providing the processing facilities. The Center for Materials Science and Engineering at MIT is acknowledged for providing the characterization facilites.

## References

1. N. Setter, D. Damjanovic, L. Eng, G. Fox, S. Gevorgian, S. Hong, A. Kingon, H. Kohlstedt, N.Y. Park, G.B. Stpehenson, I. Stolitchnov, A.K. Taganstev, D.V. Taylor, T. Yamada, S. Streiffer, J. Appl. Phys **100**, 051606 (2006)
2. Ch. Buchal, L. Beckers, A. Eckau, J. Schubert, W. Zander, Mater. Sci. Eng **B56**, 234 (1998)
3. K.J. Choi, M. Biegalski, Y.L. Li, A. Sharan, J. Schubert, R. Uecker, P. Reiche, Y.B. Chen, X.Q. Pan, V. Gopalan, L.-Q. Chen, D.G. Schlom, C.B. Eom, Science **306**, 1005 (2004)
4. O. Trithaveesak, J. Schubert, Ch. Buchal, J. Appl. Phys **98**, 114101 (2005)
5. J.S. Speck, A.C. Daykin, A. Seifert, A.E. Romanov, W. Pompe, J. Appl. Phys **78**, 1696 (1995)
6. J.H. Haeni, P. Irvin, W. Chang, R. Uecker, P. Reiche, Y.L. Li, S. Choudhury, W. Tian, M.E. Hawley, B. Craigo, A.K. Tagantsev, X. Q. Pan, S.K. Streiffer, L.Q. Chen, S.W. Kirchoefer, J. Levy, D.G. Schlom, Nature **430**, 758 (2004)
7. M.E. Lines, A.M. Glass, *Principles and Applications of Ferroelectrics and Related Materials, chap. 8* (Oxford University Press, New York, 1977)
8. B. Jaffe, W.R. Cook, H. Jaffe, *Piezoelectric Ceramics* (Academic, London and New York, 1971), p. 54
9. F. Bai, H. Zheng, H. Cao, L.E. Cross, R. Ramesh, J. Li, D. Viehland, Appl. Phys. Lett **85**, 4109 (2004)
10. Y.L. Li, L.Q. Chen, Appl. Phys. Lett **88**, 072905 (2006)
11. Y. Yoneda, T. Okabe, K. Sakaue, H. Terauchi, H. Kasatani, K. Degushi, J. Appl. Phys **83**, 2458 (1998)
12. F. He, B.O. Wells, Appl. Phys. Lett **88**, 152908 (2006)
13. B.-K. Lai, I.A. Kornev, L. Bellaiche, G.J. Salamo, Appl. Phys. Lett **86**, 132904 (2005)
14. I.B. Misirlioglu, S.P. Alpay, F. He, B.O. Wells, J. Appl. Phys **99**, 104103 (2006)
15. O. Diéguez, S. Tinte, A. Antons, C. Bungaro, J.B. Neaton, K.M. Rabe, D. Vanderbilt, Phys. Rev. B **69**, 212101 (2004)
16. N.A. Pertsev, A.G. Zembilgotov, A.K. Tagantsev, Phys. Rev. Lett **80**, 1988 (1998)
17. N.-M. Lee, T. Sekine, Y. Ito, K. Uchino, Jpn. J. Appl. Phys **33**, 1484 (1994)
18. S.B. Mi, C.L. Jia, T. Heeg, O. Trithaveesak, J. Schubert, K. Urban, J. Cryst. Growth **283**, 425 (2005)
19. H.Z. Guo, Z.H. Chen, B.L. Cheng, H.B. Lu, L.F. Liu, Y.L. Zhou, J. Eur. Cer. Soc **25**, 2347 (2005)
20. J. Zhang, D. Cui, Y. Zhou, L. Li, Z. Chen, M. Szabadi, P. Hess, Thin Solid Films **287**, 101 (1996)
21. E.J. Tarsa, E.H. Hachfeld, F.T. Quinlan, J.S. Speck, M. Eddy, Appl. Phys. Lett **68**, 490 (1996)
22. W.J. Kim, W. Chang, S.B. Qadri, J.M. Pond, S.W. Kirchoefer, D. B. Chirsey, J.S. Horwitz, Appl. Phys. Lett **76**, 1185 (2000)
23. J.A. Bellotti, W. Chang, S.B. Qadri, S.W. Kirchoefer, J.M. Pond, Appl. Phys. Lett **88**, 012902 (2006)
24. W.J. Kim, H.D. Wu, W. Chang, S.B. Qadri, J.M. Pond, S.W. Kirchoefer, D.B. Chirsey, J.S. Horwitz, J. Appl. Phys **88**, 5448 (2000)
25. H.N. Al-Shareef, D. Dimos, M.V. Raymond, R.W. Schwartz, C.H. Mueller, J. Electroceramics **1**, 145 (1997)
26. J. Lappalainen, V. Lantto, J. Frantti, J. Hiltunen, Appl. Phys. Lett **88**, 252901 (2006)
27. L. Beckers, J. Schubert, W. Zander, J. Ziesmann, A. Eckau, P. Leinenbach, Ch. Buchal, J. Appl. Phys **83**, 3305 (1998)
28. International Centre for Diffraction Data Powder Diffraction File Card No. 00-005-0626 (Newton Square, PA 1999)
29. V. Srikant, E.J. Tarsa, D.R. Clarke, J.S. Speck, J. Appl. Phys **77**, 1517 (1995)
30. M. Zgonik, P. Bernasconi, M. Duelli, R. Schlesser, P. Günter, M. H. Garrett, D. Rytz, Y. Zhu, X. Wu, Phys. Rev. B **50**, 5941 (1994)
31. X. Zhu, N. Chong, H.L.-W. Chan, C.-L. Choy, K.-H. Wong, Z. Liu, N. Ming, Appl. Phys. Lett **80**, 3376 (2002)
32. S. Rios, J.F. Scott, A. Lookman, J. McAneney, J.M. Gregg, J. Appl. Phys **99**, 024107 (2006)
33. C.B. Parker, J.-P. Maria, A. Kingon, Appl. Phys. Lett **81**, 340 (2002)
34. M. Tyunina, J. Levoska, Phys. Rev. B **70**, 132105 (2004)